

This discussion paper is/has been under review for the journal Hydrology and Earth System Sciences (HESS). Please refer to the corresponding final paper in HESS if available.

Modeling the effects of cold front passages on the heat fluxes and thermal structure of a tropical hydroelectric reservoir

M. P. Curtarelli¹, E. H. Alcântara^{1,*}, C. D. Rennó¹, and J. L. Stech¹

¹National Institute for Space Research, São José dos Campos, São Paulo, Brazil

*now at: São Paulo State University, Presidente Prudente, São Paulo, Brazil

Received: 7 June 2013 – Accepted: 25 June 2013 – Published: 2 July 2013

Correspondence to: M. P. Curtarelli (mpedroso@dsr.inpe.br)

Published by Copernicus Publications on behalf of the European Geosciences Union.

HESSD
10, 8467–8502, 2013

Modeling the effects
of cold front
passages on the heat
fluxes

M. P. Curtarelli et al.

[Title Page](#)

[Abstract](#)

[Introduction](#)

[Conclusions](#)

[References](#)

[Tables](#)

[Figures](#)



[Back](#)

[Close](#)

[Full Screen / Esc](#)

[Printer-friendly Version](#)

[Interactive Discussion](#)

Abstract

We study the influence of cold fronts on the heat fluxes and thermal structure of a tropical reservoir located in Brazil. The period chosen for this study consisted of 49 days between 28 April 2010 and 15 July 2010 and was defined based on information from the Brazilian Centre for Weather Forecasting and Climate Studies (CPTEC), data collected in situ and the interpretation of remotely sensed images. During the selected time period, five cold front passages were identified, allowing us to analyze the cumulative effect of cold fronts and the reservoir's resilience on the days that elapsed between the passages. To better understand the physical processes that drive changes in heat fluxes and thermal structure, a simulation was performed that utilized a three-dimensional hydrodynamic model. The results showed that during the cold front days, the sensible and latent heat fluxes were enhanced by approximately 24 % and 19 %, respectively. The daily average heat loss was up to 167 % higher on the cold front days than on the non-cold front days. The high heat loss and the increased wind intensity that occurred during the cold front passages destabilized the water column and provided partial or complete mixing. The colder waters of the Paranaíba River contributed to reestablish the thermal stratification following the passages of the cold fronts. These results suggest that cold front passages play an important role in the stratification and mixing regimes of Brazilian reservoirs located in southern and southeastern regions.

20 1 Introduction

Lakes and reservoirs are well known to affect the climate at different scales by affecting energy and water exchanges with the atmosphere (Krinner, 2003; Rouse et al., 2005). Reservoirs also regulate the carbon cycle, affecting the climate through the release and consumption of greenhouse gasses (Tranvik et al., 2009). It is therefore critical to understand the environmental controls on the energy, mass and gas exchanges

Title Page	
Abstract	Introduction
Conclusions	References
Tables	Figures
	
	
Full Screen / Esc	
Printer-friendly Version	
Interactive Discussion	

between reservoirs and the atmosphere to quantify their influence on climate systems (Coe, 1998; León et al., 2007; Mackay et al., 2009).

A reservoir's energy budget depends on the season and the meteorological conditions (Imberger and Patterson, 1990). Cold fronts change the weather and hence affect the reservoir's heat budget (Blanken et al., 2000; MacIntyre et al., 2009; Liu et al., 2011). Due to the cloudiness associated with these meteorological events, the shortwave solar radiation that reaches the reservoir's surface is reduced, while the longwave incoming radiation is enhanced. The sensible and latent heat loss is also enhanced, making the heat budget negative. Although the effects of cold fronts have been reported for North American water bodies, few studies have addressed this issue in South American lakes and reservoirs.

Cold front incursions are one of the most recurrent synoptic patterns over South America; they greatly affect atmospheric circulation, precipitation and temperature regimes (Garreaud, 2000). The intensities of cold front passages over South America are generally much smaller than those over North America (Marengo et al., 1997). Cold fronts occur year-round and reach the Brazilian territory every 1 to 2 weeks; however, they are more frequent during the austral wintertime (Stech and Lorenzetti, 1992). Wintertime cold fronts are also more severe and can cause freezing temperatures in South and Southeastern Brazil (Marengo et al., 2002). The majority of these fronts reach the hinterlands of São Paulo, Minas Gerais and Goiás states in which many reservoirs are located; most of these reservoirs are used to generate energy.

A preliminary investigation performed in the Itumbiara Hydroelectric Reservoir (hereafter called the Itumbiara Reservoir), which is located in Central Brazil, showed that during a cold front passage, the reservoir heat loss tends to increase in response to the changing weather conditions (Alcântara et al., 2010a). This study also demonstrated that the cold front passage contributed to water column destabilization and promoted mixing. Nevertheless, this study was limited because it utilized punctual measurements (via a monitoring buoy) and did not consider the spatial variability in the heat flux estimates. In addition, the sensible and latent heat fluxes were estimated without

Modeling the effects of cold front passages on the heat fluxes

M. P. Curtarelli et al.

[Title Page](#)

[Abstract](#)

[Introduction](#)

[Conclusions](#)

[References](#)

[Tables](#)

[Figures](#)

◀

▶

◀

▶

[Back](#)

[Close](#)

[Full Screen / Esc](#)

[Printer-friendly Version](#)

[Interactive Discussion](#)

Modeling the effects of cold front passages on the heat fluxes

M. P. Curtarelli et al.

[Title Page](#)

[Abstract](#)

[Introduction](#)

[Conclusions](#)

[References](#)

[Tables](#)

[Figures](#)



[Back](#)

[Close](#)

[Full Screen / Esc](#)

[Printer-friendly Version](#)

[Interactive Discussion](#)

considering the stability of the atmospheric boundary layer (ABL), which is persistently unstable over tropical reservoirs (Verburg and Antenucci, 2010), leading to underestimated heat fluxes.

An efficient approach that has been widely used to support and complement the understanding of physical processes in lakes and reservoirs is the use of a three-dimensional (3-D) hydrodynamic model (Vidal et al., 2007; Rueda and MacIntyre, 2009; Okely et al., 2010). One advantage of this approach is that it can simulate, in the space and time, real and hypothetical scenarios; it can also simulate various physical processes simultaneously (Rajar and Cetina, 1997). Conversely, one of the major disadvantages is the large amount of input data and parameters required, which often limits its use (Bonnet and Wessen, 2001).

To overcome the lack of in situ data for the input, calibration and validation of models, some authors have utilized a synergistic approach that integrates remote sensing techniques and numerical modeling (Hedger et al., 2002; Pleskachevsky et al., 2005). The availability of remote sensing data at different temporal and spatial resolutions allows new approaches and methodologies for monitoring the water quality and the energy balance in inland water bodies (Kutser et al., 2005; Alcântara et al., 2010b). The advantages of using remote sensing data to investigate inland water bodies are the synoptic view of large areas, spatial variability of data and repetitive data acquisition (Jensen, 2006). Moreover, the cost of data acquired by sensors onboard orbital platforms can be lower than the data acquired by conventional methods (discounting the cost of the satellites) (Jensen, 2006).

For the reasons described above, this study aimed to investigate the effects of cold front passages on the heat fluxes and thermal structure of a tropical reservoir located in Brazil. To gain a better understanding of these processes, we conducted simulations with a 3-D hydrodynamic model that was supported by in situ and remotely sensed data.

2 Site description

The Itumbiara Reservoir is located in the Paraná River basin ($18^{\circ}25' S$, $49^{\circ}06' W$) at the border of the Minas Gerais and Goiás States, Central Brazil (Fig. 1a). The reservoir was formed by the damming of the Paranaíba River, which resulted in the flooding of its main tributaries, the Corumbá and Araguari Rivers. The basin's geomorphology resulted in a lake with a dendritic pattern covering an area of approximately 778 km^2 and a volume of $17.03 \text{ billion m}^3$. The reservoir's surface is located 520 m a.s.l. (meters above sea level). The major axis is 30 km long, and the maximum width is approximately 15 km . The reservoir depth ranges from 0.5 m to 78 m , with a mean depth of 32 m (Fig. 1b).

According to the Köppen classification system (Donn, 1978), the climate in the Itumbiara Reservoir region is classified as “tropical savanna” with two well-defined seasons, dry (May–October) and wet (December–April). The monthly precipitation ranges from 5 mm in the peak of the dry season (winter in the Southern Hemisphere) to 250 mm in the peak of the wet season (summer in Southern Hemisphere). The average air temperature is higher during the wet season (24°C to 26°C) and then decreases during the dry season, reaching values lower than 20°C in July. The relative humidity displays a pattern similar to that of the air temperature but with a small shift in the minimum value toward September (47 %). The wind intensity is lower during the wet season (1.6 m s^{-1}) than in the dry season (3.3 m s^{-1}). On average, 11 cold fronts pass over the reservoir annually; approximately 75 % of the occurrences are during the dry season (Curtarelli, 2012). May and September contain the highest frequencies of cold front passages, with two passages each on average. Depending on its intensity, a cold front can remain over the Itumbiara Reservoir for up to five days (Curtarelli, 2012).

Modeling the effects of cold front passages on the heat fluxes

M. P. Curtarelli et al.

[Title Page](#)

[Abstract](#)

[Introduction](#)

[Conclusions](#)

[References](#)

[Tables](#)

[Figures](#)



[Back](#)

[Close](#)

[Full Screen / Esc](#)

[Printer-friendly Version](#)

[Interactive Discussion](#)

3 Data and methods

3.1 Reservoir bathymetry

The bathymetry of the Itumbiara Reservoir was derived from depth samples collected with an LMS-525 Lowrance® ecobathymeter (Tulsa, OK, USA) during two field campaigns conducted in May and August 2009. A total of 125 631 depth samples, with accuracy of ± 0.1 m, were collected during the two field campaigns. The bathymetric grid with a spatial resolution of 150 m \times 150 m was obtained by interpolating the depth samples using an ordinary Kriging algorithm (Bailey and Gretel, 1995) following the approach described by Merwade (2009). The depth values were corrected to the maximum level of reservoir operation (520 m a.s.l.).

3.2 Field data

The field dataset used in this study includes meteorological, limnological and fluvio-metric data. The meteorological data were acquired by two autonomous “SIMA” (Integrated System for Environment Monitoring, Stech et al., 2006) systems that were anchored within the reservoir (see the location in Fig. 1). SIMA is a set of hardware and software designed for meteorological and limnological data acquisition and real-time monitoring of natural and artificial aquatic systems. It is composed of an independent system, consisting of an anchored buoy, containing a fixed payload (sensors, data storage systems, transmission antenna and a battery). The meteorological sensors are fixed 3 m above the water surface. The data are collected at preprogrammed time intervals (hourly for the Itumbiara Reservoir) and are transmitted by satellites in quasi-real-time; they are available to any user located within 2500 km of the acquisition point. The primary characteristics of the SIMA sensors used in this work are summarized in Table 1. Further information about SIMA conception and operation can be found online: <http://www.dsr.inpe.br/hidrosfera/sima/en/>. Throughout this paper, the

[Title Page](#)

[Abstract](#)

[Introduction](#)

[Conclusions](#)

[References](#)

[Tables](#)

[Figures](#)



[◀](#)

[▶](#)

[Back](#)

[Close](#)

[Full Screen / Esc](#)

[Printer-friendly Version](#)

[Interactive Discussion](#)

SIMA located near the dam will be called station S1, while that anchored near the river–reservoir transition zone will be called station S2.

Water temperature data at different depths were collected by thermistor chains coupled to the SIMA. The S1-coupled thermistor chain collected temperature data at five depths (1, 5, 12, 20 and 40 m), while the S2-coupled thermistor chain collected temperature data at three depth (5, 12 and 20 m). The thermistors are accurate to $\pm 0.20\text{ }^{\circ}\text{C}$ and have a response time of 2.5 s (when suspended by their leads in a well-stirred oil bath). Water temperature data were collected hourly and sent via a satellite downlink to a ground station in near-real-time.

The time series of total inflow, outflow and water level measured daily were provided by Eletrobrás–Furnas (<http://www.furnas.com.br/Ingles/index.aspx>), which is the company that oversees the reservoir's operation. The total inflow was divided between the two main tributaries (Paranaíba and Corumbá River) based on outflow time series of the Corumbá Reservoir, which is located in the Corumbá River at a location 35 km upstream of the Itumbiara Reservoir. Because the Corumbá Reservoir is located relatively close to the Itumbiara Reservoir, we assumed that the Corumbá River inflow was equal to the Corumbá Reservoir outflow. The Paranaíba River inflow was calculated by subtracting the Corumbá River inflow from the total inflow. We estimated that 79 % of the total inflow is attributed to the Paranaíba River, and 21 % is attributed to the Corumbá River. Then, the total inflow data were distributed between the two inflows using the percentages indicated above.

3.3 Satellite data

The satellite-based dataset used in this study includes cloud cover, the water surface temperature (WST) of the rivers' inflows and the daily precipitation rates over the Itumbiara Reservoir. The cloud cover and WST used in this study are standard products (named M*D35L2 and M*D11A1, respectively) that were retrieved from a dataset collected by the Moderate Resolution Imaging Spectroradiometer (MODIS) (Justice et al., 1998). Both the M*D35L2 and M*D11A1 products are generated up to four times

[Title Page](#)

[Abstract](#)

[Introduction](#)

[Conclusions](#)

[References](#)

[Tables](#)

[Figures](#)

◀

▶

◀

▶

[Back](#)

[Close](#)

[Full Screen / Esc](#)

[Printer-friendly Version](#)

[Interactive Discussion](#)

**Modeling the effects
of cold front
passages on the heat
fluxes**

M. P. Curtarelli et al.

[Title Page](#)[Abstract](#)[Introduction](#)[Conclusions](#)[References](#)[Tables](#)[Figures](#)[Back](#)[Close](#)[Full Screen / Esc](#)[Printer-friendly Version](#)[Interactive Discussion](#)

each day (i.e., 10:30 LT, 13:30 LT, 23:30 LT and 02:30 LT) and are delivered in a georeferenced grid with 1 km of spatial resolution in a sinusoidal projection. More information about the MODIS WST and cloud cover products can be found in Wan (2008) and Ackerman et al. (1998), respectively.

- 5 The MODIS products were acquired online (<http://reverb.echo.nasa.gov/reverb/>) and were preprocessed using the MODIS Reprojection Tool (available at https://lpdaac.usgs.gov/tools/modis_reprojection_tool). The data were first resampled to a 150 m spatial resolution (compatible with the bathymetric grid). They were then re-projected to the Universal Transverse Mercator (UTM) coordinate system (zone 22 South) with the
10 World Geodetic System (WGS-84) datum as reference; they were then converted to a raster image. A MATLAB® program was then used to retrieve the WST at the rivers' inflows and the cloud cover time series over the Itumbiara Reservoir.

- The precipitation rates were provided by Tropical Rainfall Satellite Measuring Mission (TRMM) (Kummerow et al., 1998), which is a satellite dedicated to monitoring the
15 precipitation in Earth's tropical regions. In this study, we used the TRMM 3B42 product version 6, which provides 3 h accumulated precipitation rates in a georeferenced grid with 25 km resolution. The precipitation time series over the Itumbiara Reservoir was generated using the TRMM Online Visualization and Analysis System (TO-VAS), which is available online (http://gdata1.sci.gsfc.nasa.gov/daac-bin/G3/gui.cgi?instance_id=TRMM_3-Hourly). More details about the TRMM 3B42 version 6 product
20 can be found online (<http://trmm.gsfc.nasa.gov/3b42.html>).

3.4 Model description

- The Estuary and Lake Computational Model (ELCOM) (Hodges et al., 2000) was used to simulate the response of the Itumbiara Reservoir to the cold front passages.
25 ELCOM solves unsteady, coupled, Reynolds-Averaged Navier–Stoke equations and scalar transport equations using hydrostatic and Boussinesq approximations to model the velocity, salinity and temperature of water in 3-D space and time. The hydrodynamic algorithms that are implemented in ELCOM use an Euler–Lagrange approach

for the advection of momentum adapted from the work of Casulli and Cheng (1992), while the advection of scalars (i.e., tracers, salinity and temperature) are based on the ULTIMATE QUICKEST method proposed by Leonard (1991).

The thermodynamics model considers the penetrative (i.e., shortwave radiation, Q_{sw}) and non-penetrative components (i.e., longwave radiation, Q_{lw} , sensible, Q_{sh} , and latent, Q_{lh} , heat fluxes) (Hodges et al., 2000). The fraction of Q_{sw} (280 nm to 2800 nm) that penetrates into the water body, $Q_{\text{sw}}^{(-0)}$ (W m^{-2}), is given by:

$$Q_{\text{sw}}^{(-0)} = Q_{\text{sw_total}} (1 - r_a^{\text{sw}}) \quad (1)$$

where $Q_{\text{sw_total}}$ is the total incident shortwave radiation over the water surface (W m^{-2}) and r_a^{sw} is the albedo of water for shortwave radiation. ELCOM allows the user to divide the $Q_{\text{sw_total}}$ into four components (photosynthetically active radiation (PAR), near-infrared and ultraviolet A and B); the attenuation through the water column follows the Beer–Lambert Law:

$$Q_{\text{sw}}(z) = Q_{\text{sw}}^{(-0)} e^{-\eta_a z} \quad (2)$$

where z is the depth below the water surface (m) and η_a is the shortwave attenuation coefficient (m^{-1}). The net Q_{lw} (W m^{-2}) can be estimated based on the cloud cover fraction, C , as follows:

$$Q_{\text{lw}} = \left(1 - r_a^{(\text{lw})}\right) (1 + 0.17C^2)\varepsilon_a\sigma T_a^4 - \varepsilon_s\sigma T_s^4 \quad (3)$$

where $r_a^{(\text{lw})}$ is the water albedo for the longwave radiation, ε_a is the air emissivity, σ is the Stefan–Boltzmann constant ($= 5.6697 \times 10^{-8} \text{ W m}^{-2} \text{ K}^{-4}$), T_a is the air temperature ($^\circ\text{C}$), ε_s is the water emissivity ($= 0.96$), and T_s is the water surface temperature ($^\circ\text{C}$). Q_{sh} (W m^{-2}) and Q_{lh} (W m^{-2}) are estimated by standard bulk transfer models and are parameterized as functions of meteorological variables as described by Fischer et al. (1979):

$$Q_{\text{sh}} = C_{\text{sh}}\rho_a c_p U_{10} (T_a - T_s) \quad (4)$$

Modeling the effects of cold front passages on the heat fluxes

M. P. Curtarelli et al.

[Title Page](#)

[Abstract](#)

[Introduction](#)

[Conclusions](#)

[References](#)

[Tables](#)

[Figures](#)



[Back](#)

[Close](#)

[Full Screen / Esc](#)

[Printer-friendly Version](#)

[Interactive Discussion](#)

$$Q_{lh} = \frac{0.622}{p} C_{lh} \rho_a L_E U_{10} (e_a - e_s) \quad (5)$$

where C_{sh} is the transfer coefficient for sensible heat flux, ρ_a is the air density (kg m^{-3}), c_p is the specific heat of air at a constant pressure ($= 1003 \text{ J kg}^{-1} \text{ K}^{-1}$), U_{10} is the wind

- 5 speed (m s^{-1}) at the standard reference height of 10 m, p is the atmospheric pressure (mbar), C_{lh} is the transfer coefficient for latent heat flux (J kg^{-1}), e_a is the vapor pressure of the air (mbar), and e_s is the saturation vapor pressure (mbar) at T_s . ELCOM does not consider the condensation effects in its formulation. Furthermore, ELCOM allows the user to simulate the effects of atmospheric stability on the surface heat fluxes using the
- 10 iterative procedure proposed by Hicks (1975) and described by Imberger and Patterson (1990). In this case, the extrapolation of meteorological data collected at a given height above the water surface to the 10 m standard reference height is done following Rayner (1981).

- The vertical mixing model uses the transport equations of turbulent kinetics energy (TKE) to compute the energy available from wind stirring and shear production for the mixing process (Spiegel and Imberger, 1980). The energy required to occur vertical mixture is given by the density gradient in the water column. The wind energy available for mixing, E_{wind} (J kg^{-1}), is parameterized as a function of the wind shear velocity, u_* (m s^{-1}), and a mixing coefficient, C_n ($= 1.33$), as follows:

$$20 \quad E_{wind} = \frac{1}{2} C_n^3 u_*^3 \quad (6)$$

The shear energy, E_{shear} (J kg^{-1}), is parameterized as a function of shear, S (m s^{-1}), and another mixing coefficient, C_S ($= 0.15$), as follows:

$$E_{shear} = \frac{1}{2} C_S S^2 \quad (7)$$

Modeling the effects of cold front passages on the heat fluxes

M. P. Curtarelli et al.

[Title Page](#)

[Abstract](#)

[Introduction](#)

[Conclusions](#)

[References](#)

[Tables](#)

[Figures](#)

◀

▶

◀

▶

[Back](#)

[Close](#)

[Full Screen / Esc](#)

[Printer-friendly Version](#)

[Interactive Discussion](#)

Modeling the effects of cold front passages on the heat fluxes

M. P. Curtarelli et al.

[Title Page](#)

[Abstract](#)

[Introduction](#)

[Conclusions](#)

[References](#)

[Tables](#)

[Figures](#)

[◀](#)

[▶](#)

[◀](#)

[▶](#)

[Back](#)

[Close](#)

[Full Screen / Esc](#)

[Printer-friendly Version](#)

[Interactive Discussion](#)

The TKE generated due to drag on the reservoir's bottom can be included in the mixing model according to the boundary condition set by the user. A complete description of the formulae and numerical methods used in ELCOM was described by Hodges et al. (2000).

5 3.5 Period of simulation

The period of 6 May 2010 to 15 July 2010 was chosen to simulate the cold front passage effects on the heat budget and in the stratification and mixing processes of the Itumbiara Reservoir. This period was chosen based on the availability of reliable in situ and remote sensing data and the occurrence of cold fronts. According to 10 the CPTEC/INPE climate report (available at <http://climanalise.cptec.inpe.br/~rclimanl/boletim/>), five cold fronts (hereafter referred as F1, F2, F3, F4 and F5) passed over the Itumbiara region during the period selected. These five cold front passages were confirmed by analyzing the meteorological data collected in situ and from satellite images (Fig. 2). Table 2 shows a summary of the weather condition changes that occurred 15 during the cold front passages and the period of cold front activity over the Itumbiara Reservoir.

3.6 Model setup and validation

The numerical domain, which was based on the bathymetry data availability, was discretized in a uniform horizontal grid containing $150\text{ m} \times 150\text{ m}$ cells. The vertical grid 20 resolution was set to a uniform 1 m thickness, resulting in 78 vertical layers. The horizontal and vertical resolutions were carefully chosen to optimize model performance and to reduce computational cost. The water albedo was set to 0.03 (Slater, 1980), and the bottom drag coefficient was set to 0.001 (Wüest and Lorke, 2003). The attenuation coefficient for PAR was set to 0.6 m^{-1} based on Secchi disc measurements 25 performed in the Itumbiara Reservoir during a field survey conducted in May 2009. A value of $5.25\text{ m}^2\text{s}^{-1}$, which was based on a previous study conducted in another

Modeling the effects of cold front passages on the heat fluxes

M. P. Curtarelli et al.

[Title Page](#)

[Abstract](#)

[Introduction](#)

[Conclusions](#)

[References](#)

[Tables](#)

[Figures](#)



[Back](#)

[Close](#)

[Full Screen / Esc](#)

[Printer-friendly Version](#)

[Interactive Discussion](#)

tropical reservoir (Pacheco et al., 2011), was chosen for the horizontal diffusivity for temperature and for the horizontal momentum.

Due to the presence of persistent unstable atmospheric conditions over tropical reservoirs (Verburg and Antenucci, 2010), the atmospheric stability sub-model was activated during the simulation; this procedure is appropriate in the cases in which the meteorological sensors are located within the internal boundary layer over the surface of the lake and data is collected at sub-daily intervals (Imberger and Patterson, 1990). In this manner, at each model time step the heat and momentum transfer coefficients were adjusted based on the stability of the ABL. The stability of ABL is verified through the Monin–Obukhov length scale.

We defined three sets of boundary cells to force the inflow and outflow: two inflows (the Corumbá and Paranaíba Rivers) and one outflow (the water intake at the bottom of the dam). The free surface of the reservoir was divided into two sections: one was under the influence of S1, and the other was under the influence of the S2 meteorological dataset. The model was forced using hourly meteorological data acquired by the two SIMAs, the daily inflow and outflow provided by Eletrobrás–Furnas, the cloud cover and river temperatures extracted from the MODIS products and the daily precipitation provided by the TRMM 3B42 product (Fig. 3).

To provide realistic estimates, the simulation was initiated 8 days before the period of interest to spin-up the circulation patterns and water temperature gradient (see Fig. 3). The simulation began on 28 April 2010 at 23:30 LT and finished on 15 July 2010 at 23:30 LT. All the time used in this work is referred to the local time (LT, –3 UTC). The simulation was programmed to run at efficient time steps with the Courant–Friedrichs–Lewy number fixed at 1/3 (Hodges et al., 2006). Thus, the time step was set to 150 s, which was sufficient to ensure the numerical stability of the model (Cassulli and Cattani, 1994). The initial temperature profiles were defined using the data collected by the two thermistor chains. The free surface was considered to be flat at the beginning of the simulation, and the water level was at 517 m a.s.l. The results were preprogrammed to be recorded at every 12 time steps (i.e., 30 min).

Title Page	
Abstract	Introduction
Conclusions	References
Tables	Figures
◀	▶
◀	▶
Back	Close
Full Screen / Esc	
Printer-friendly Version	
Interactive Discussion	

The ELCOM results were validated using the water temperature data acquired hourly by the thermistor chains at stations S1 and S2 and the water level data that were measured daily at the dam. The validation was performed in the following three different ways: (1) a visual comparison of the position of the isotherms obtained using field data and estimated by the model; (2) error analysis of simulated water temperatures at different depths (the same depths as the thermistor chains); and (3) error analysis of the simulated water level near the dam.

4 Results and discussion

4.1 Meteorological forcing at the Itumbiara Reservoir

A marked diel pattern was observed for air temperature, shortwave radiation, humidity and wind speed (Fig. 3a–d). During the days on which cold fronts did not pass, the air temperature typically ranged from 20 °C to 30 °C, with the lowest temperature values observed at approximately 09:00 LT and the higher values observed at approximately 18:00 LT. The shortwave radiation peak (approximately 800 W m^{-2}) occurred at approximately noon. On average, the humidity ranged from 45 % to 75 %, with the higher values observed during the morning. The lowest humidity was observed during the afternoon at approximately 19:00 LT. The wind speed was higher in the morning, reaching 6 m s^{-1} with a preferential direction coming from the NE.

However, during the cold front days, the air temperature decreased, typically ranging from 15 °C to 22 °C. Due to the cloudiness associated with the cold front passages over the Itumbiara Reservoir (Fig. 3e), the shortwave radiation peaks were lower during the cold front days; in some cases the maximum shortwave radiation observed was 250 W m^{-2} . The relative humidity also decreased during the cold front passage days, reaching values of approximately 30 %. The wind speed increased, reaching values of approximately 9 m s^{-1} , and the preferential wind direction changed to the S or SW.

4.2 Model validation

Figure 4 shows the observed and simulated temperatures for the Itumbiara Reservoir. Figure 4a, b presents the results for point S1, located near the dam, and the Fig. 4c, d presents the results for point S2, located in the river–reservoir transition zone. At both analyzed points, the model was able to reasonably reproduce the thermal structure. Visually, the isotherms and the diurnal cycle of stratification were also well-represented by the model.

The error analysis of the simulated temperature (Table 3) showed that for both sampled validation points and depths, the Root-Mean-Square-Error (RMSE) was lower than 3 %, indicating that ELCOM performed well when predicting the water column temperature. The model performed better in the region near the dam, with an average RMSE of $0.34\text{ }^{\circ}\text{C}$ (1.3 % of range); the validation point in the river–reservoir transition zone had an average RMSE of $0.66\text{ }^{\circ}\text{C}$ (1.96 % of range). This level of accuracy is consistent with other 3-D modeling studies in lakes (Hodges et al., 2000; Okely et al., 2010). The error analysis of the simulated water level near the dam also produced favorable results ($\text{RMSE} < 1\text{ \%}$), indicating that the ELCOM model could compute the water balance and represent the reduction in the water level during the simulation period very well.

4.3 Surface heat fluxes

All three components of the surface heat fluxes showed a marked diel cycle (Fig. 5a); the peak heat loss occurred between 01:00 LT and 05:00 LT. The latent heat flux was the primary component of the surface heat flux; on average, it accounted for 64 % of the daily loss. On the days on which cold fronts were absent, the latent heat flux ranged, on average, from -64 W m^{-2} to -292 W m^{-2} . On the cold front days, the latent heat flux increased and ranged, on average, from -150 W m^{-2} to -300 W m^{-2} ; however, in some cases, the flux exceeded -400 W m^{-2} . The maximum loss was observed during F2, when the latent heat flux reached -491 W m^{-2} . This value is approximately 1.5-fold higher than the maximum latent heat loss observed during a non-cold front day. The

[Title Page](#)[Abstract](#)[Introduction](#)[Conclusions](#)[References](#)[Tables](#)[Figures](#)[◀](#)[▶](#)[◀](#)[▶](#)[Back](#)[Close](#)[Full Screen / Esc](#)[Printer-friendly Version](#)[Interactive Discussion](#)

Modeling the effects of cold front passages on the heat fluxes

M. P. Curtarelli et al.

[Title Page](#)

[Abstract](#)

[Introduction](#)

[Conclusions](#)

[References](#)

[Tables](#)

[Figures](#)

◀

▶

◀

▶

[Back](#)

[Close](#)

[Full Screen / Esc](#)

[Printer-friendly Version](#)

[Interactive Discussion](#)

4.4 Heat budget

The heat budget (Fig. 5c) was primarily controlled by the shortwave incoming radiation and the latent heat flux. Heat gain occurred during the morning and the afternoon, between 09:00 LT and 18:00 LT, and heat loss occurred for the remainder of the day. During the non-cold front days, the heat budget ranged, on average, from 450 Wm⁻² to -400 Wm⁻². On the cold front days, the heat budget ranged, on average, from 230 Wm⁻² to -450 Wm⁻²; however, it exceeded -500 Wm⁻² in some cases. The maximum heat loss was observed on 12 May at 19:00 LT during F2, when the heat budget was -611 Wm⁻². This value is approximately 2-fold higher than the maximum heat loss observed during a non-cold front day.

The daily averaged heat budget ranged from 145 Wm⁻² to -249 Wm⁻², with a mean value of -41 Wm⁻². Considering only the days with cold front passages, the daily averaged heat budget was approximately -74 Wm⁻², representing an increase of 167 % (in absolute value) when compared with the days lacking cold front passages (-28 Wm⁻² on average).

4.5 Water column thermal structure

Figure 6 shows the temporal variation of the thermal structure along the longitudinal transect of the Itumbiara Reservoir (the transect is shown in Fig. 1). At the beginning of the simulated period (i.e., the beginning of the dry season), the main body of the Itumbiara Reservoir was stratified with a difference of 2 °C between the surface (28.5 °C) and the bottom (26.5 °C). The permanent thermocline was localized at approximately 30 m depth and was tilted toward the river–reservoir transition zone. A marked diel cycle of stratification was observed, and the diurnal mixed layer formed between 12:00 LT and 20:00 LT. The maximum value of the diel cycle of stratification occurred at approximately 16:00 LT, with the diurnal mixed layer reaching 5 m depth (Fig. 6a). During the passage of F1, the increased wind intensity and heat loss promoted the deepening of the thermocline (Fig. 6b); however, the water column was

[Title Page](#)[Abstract](#)[Introduction](#)[Conclusions](#)[References](#)[Tables](#)[Figures](#)[◀](#)[▶](#)[Back](#)[Close](#)[Full Screen / Esc](#)[Printer-friendly Version](#)[Interactive Discussion](#)

Modeling the effects of cold front passages on the heat fluxes

M. P. Curtarelli et al.

[Title Page](#)

[Abstract](#)

[Introduction](#)

[Conclusions](#)

[References](#)

[Tables](#)

[Figures](#)

◀

▶

◀

▶

[Back](#)

[Close](#)

[Full Screen / Esc](#)

[Printer-friendly Version](#)

[Interactive Discussion](#)

incompletely mixed. After the passage of F1, the permanent thermocline deepened to a 40 m depth (Fig. 6c), but the main body of the reservoir remained weakly stratified. With only one day elapsing between the passages of F1 and F2, the reservoir had little time to reestablish the thermocline, which was partially eroded during the passage of

5 F2 due to the large amount of energy released (Fig. 6d). Following F2 (Fig. 6e), the main reservoir body was partially mixed, and the difference between the surface and bottom temperatures was less than 1 °C near the dam.

This temperature difference was greater toward the river–reservoir transition zone (~ 1.5 °C), indicating that the river temperature exerted some influence on the thermal 10 structure of the reservoir, thus contributing to water column stability. During the passage of F3 (Fig. 6f), the diurnal mixed layer was not formed, and the water column was completely mixed in the majority of the reservoir. However, after the passage of F3, a period of 10 days elapsed in which cold front passages did not occur; therefore, 15 the stratification was partially reestablished in the main body of the reservoir (Fig. 6g). This stratification remained until the passage of F4 (Fig. 6h), when the thermocline was again eroded.

Upwelling events were observed following the F4 passage (Fig. 6i). During the F5 passage (Fig. 6j), the water column was totally mixed in the main body of the reservoir, but it was only partially mixed in the transition zone. Due to the influence of the 20 Paranaíba River water temperature, which is colder than the reservoir temperature, a few days after the last cold front passage (Fig. 6k, l), the reservoir was partially re-stratified; the difference between the surface and bottom temperatures reached 2.5 °C in the transition zone.

4.6 Cold front effects on stratification and mixing processes

25 Similar to other tropical lakes (MacIntyre et al., 2002), the Itumbiara Reservoir undergoes a diel cycle of stratification and mixing. To analyze the effects of cold front

passages on the water column stability, we computed the Brunt–Väisälä frequency, N^2 , (Pond and Pickard, 1983) as follows:

$$N^2 = - \left(\frac{g}{\rho_0} \right) \frac{d\rho}{dz} \quad (8)$$

where g is acceleration due to gravity ($= 9.81 \text{ m s}^{-2}$), ρ_0 is the reference density (kg m^{-3}), and ρ is the water density (kg m^{-3}). We also computed the Lake number, L_N , (Imberger and Patterson, 1990) as follows:

$$L_N = \frac{g S_t (1 - z_t/z_m)}{\rho_s u_*^2 \sqrt{A_m} (1 - z_g/z_m)} \quad (9)$$

where z_t is the height from the reservoir bottom to the center of the thermocline, z_m is the maximum reservoir depth ($= 78 \text{ m}$), ρ_s is the density of the reservoir surface water (kg m^{-3}), A_m is the reservoir surface area (m^2), z_g is the center of volume of the reservoir (m), and S_t is Schmidt stability, which is calculated as follows:

$$S_t = \frac{1}{A_m} \int_0^{z_m} (z - z_g) A(z) \rho(z) dz \quad (10)$$

where z is the vertical upward coordinate (m), $A(z)$ is the area of the reservoir at height z (m^2), $\rho(z)$ is the water density at height z (kg m^{-3}), and z_g is the center of volume of the reservoir (m), which is calculated as follows:

$$z_g = \frac{\int_0^{z_m} z A(z) dz}{\int_0^{z_m} A(z) dz} \quad (11)$$

N^2 represents the angular frequency at which a vertically displaced parcel of fluid will oscillate within a statically stable environment. Conversely, L_N characterizes the dynamic stability of a lake and represents the ratio between moments of the wind force

Modeling the effects of cold front passages on the heat fluxes

M. P. Curtarelli et al.

[Title Page](#)

[Abstract](#)

[Introduction](#)

[Conclusions](#)

[References](#)

[Tables](#)

[Figures](#)



[Back](#)

[Close](#)

[Full Screen / Esc](#)

[Printer-friendly Version](#)

[Interactive Discussion](#)



Modeling the effects of cold front passages on the heat fluxes

M. P. Curtarelli et al.

[Title Page](#)

[Abstract](#)

[Introduction](#)

[Conclusions](#)

[References](#)

[Tables](#)

[Figures](#)

◀

▶

◀

▶

[Back](#)

[Close](#)

[Full Screen / Esc](#)

[Printer-friendly Version](#)

[Interactive Discussion](#)

at the surface of the lake and the gravity-restoring force due to the stratification, above the center of the reservoir volume (Imberger and Patterson, 1990).

The high heat loss that occurred due to the passages of cold fronts over the Itumbiara Reservoir affected the water column temperature and stability. Prior to the passage of the first cold front, the water column presented a temperature difference of 2.5°C between the surface and the bottom; following the passage of the cold front, the water temperature of the surface layer and the temperature difference in the water column decreased. The analysis of L_N is shown in Fig. 7a, b. When $L_N > 1$, no deep upwelling occurs, and when $L_N < 1$, the cold deep, often nutrient-rich water from the hypolimnion reaches the surface layer during the wind episode (Antenucci and Imberger, 2003). For L_N values as high as 60, little turbulent mixing is expected in the hypolimnion (Hondzo and Stefan, 1996).

In this case, all instances for which $L_N > 1$ occurred during the daytime, when incident shortwave radiation was present; however, following the passage of a cold front, the L_N values increased during the heating phase. Often, $L_N < 1$ occurred during the nighttime; the unique exception is the day during which the cold front passage resulted in $L_N < 1$. Following the passage of a front, the water from the hypolimnion becomes progressively cooler, and the mixed layer moves to the top layer. The increased L_N value following the passage of the daytime front may be explained because during the passage of a cold front, the water loses energy to the atmosphere, and when the cold front dissipates, the incident shortwave radiation heats the surface, creating a condition that enhances the stability of the water column.

The Brunt–Väisälä frequency (Fig. 7c, d) shows that prior to the cold front passage, the stratification was stable ($N^2 > 0$) during the daytime and less stable during the nighttime. During the cold front passage, the stability of the stratification was destroyed and the system mixed ($N^2 = 0$). Following the cold front passage, the system returned to stable stratification during the day and vertical mixing at night. The Brunt–Väisälä frequency shows that the depth of mixed layer is approximately 20 m ($N^2 = 0$). In very few cases, the mixed layer depths reached 40 m; when this phenomenon occurs, the

water column overturns. This complete vertical mixing erodes the barrier imposed by the stratification (more commonly during the day prior to a cold front) and facilitates the availability of nutrient-rich, deep waters that increase primary production (Ostrovsky et al., 1996).

5 4.7 Effect of atmospheric stability on the heat budget

During the simulated period, the ABL over the Itumbiara Reservoir was unstable for 98 % of the time. This persistent unstable condition results in substantially increased heat loss for tropical reservoirs and lakes (Verburg and Antenucci, 2010). For the Itumbiara Reservoir, the unstable ABL increased the heat transfer coefficients by 49 %
10 relative to the transfer coefficients obtained considering the ABL neutral; the coefficients changed from 0.00143 to 0.00220. These values are similar to those reported by Verburg and Antenucci (2010) for Lake Tanganyika, Africa. As result of the increased heat transfer coefficients due to the unstable ABL, the Q_{sh} and Q_{lh} losses were enhanced by approximately 23 % and 13 %, respectively, when compared with the fluxes
15 estimated considering the ABL neutral. The impact on Q_{total} was approximately 24 % (26 W m^{-2}), representing a difference of 0.02 PW (1 PW = 10^{15} W) of energy released by the reservoir during the analyzed period.

5 Conclusions

We investigated the effects of successive cold front passages on the heat fluxes and thermal structure of a tropical reservoir located in Brazil combining 3-D hydrodynamic modeling, remote sensing and in situ data. The main conclusions are:
20

The cold front passages lead to significant changes in meteorological conditions over Itumbiara Reservoir that largely promote turbulent mixing through increased vertical gradients of temperature and vapor pressure between the water surface and the ABL as well as increased wind speeds. Hence, the surface energy budget rates were
25

[Title Page](#)

[Abstract](#)

[Introduction](#)

[Conclusions](#)

[References](#)

[Tables](#)

[Figures](#)



[Back](#)

[Close](#)

[Full Screen / Esc](#)

[Printer-friendly Version](#)

[Interactive Discussion](#)

Modeling the effects of cold front passages on the heat fluxes

M. P. Curtarelli et al.

[Title Page](#)

[Abstract](#)

[Introduction](#)

[Conclusions](#)

[References](#)

[Tables](#)

[Figures](#)



[Back](#)

[Close](#)

[Full Screen / Esc](#)

[Printer-friendly Version](#)

[Interactive Discussion](#)



References

Modeling the effects of cold front passages on the heat fluxes

M. P. Curtarelli et al.

- Ackerman, S. A., Strabala, K. I., Menzel, W. P., Frey, R. A., Moeller, C. C., and Gumley, L. E.: Discriminating clear-sky from clouds with MODIS, *J. Geophys. Res.*, 103, 32141–32173, 1998.
- 5 Alcântara, E. H., Bonnet, M. P., Assireu, A. T., Stech, J. L., Novo, E. M. L. M., and Lorenzzetti, J. A.: On the water thermal response to the passage of cold fronts: initial results for Itumbiara reservoir (Brazil), *Hydrol. Earth Syst. Sci. Discuss.*, 7, 9437–9465, doi:10.5194/hessd-7-9437-2010, 2010a.
- 10 Alcântara, E. H., Stech, J. L., Lorenzzetti, J. A., Bonnet, M.-P., Casamitjana, X., Assireu, A. T., and Novo, E. M. L. M.: Remote sensing of water surface temperature and heat flux over a tropical hydroelectric reservoir, *Remote Sens. Environ.*, 114, 2651–2665, 2010b.
- Antenucci, J. and Imberger, J.: The seasonal evolution of wind/internal wave resonance in Lake Kineret, *Limnol. Oceanogr.*, 48, 2055–2061, 2003.
- Bailey, T. C. and Gatrell, A. C.: Interactive Spatial Data Analysis, Prentice Hall, Harlow, 1995.
- 15 Blanken, P. D., Rouse, W. R., Culf, A. D., Spence, C., Boudreau, L. D., Jasper, J. N., Kochtubadja, B., Schertzer, W. M., Marsh, P., and Verseghy, D.: Eddy covariance measurements of evaporation from Great Slave Lake, Northwest Territories, Canada, *Water Resour. Res.*, 36, 1069–1077, 2000.
- Bonnet, M.-P. and Wessen, K.: ELMO, a 3-D water quality model for nutrients and chlorophyll: first application on a lacustrine ecosystem, *Ecol. Model.*, 141, 19–33, 2001.
- 20 Casulli, V. and Cattani, E.: Stability, accuracy and efficiency of a semi-implicit method for three-dimensional shallow water flow, *Comput. Math. Appl.*, 27, 99–112, 1994.
- Casulli, V. and Cheng, R. T.: Semi-implicit finite difference methods for three-dimensional shallow water flow, *Int. J. Numer. Meth. Fl.*, 15, 629–648, 1992.
- 25 Coe, M. T.: A linked global model of terrestrial hydrological processes: Simulation of modern rivers, lakes, and wetlands, *J. Geophys. Res.*, 103, 8885–8899, 1998.
- Curtarelli, M. P.: Study of the Influence of Cold Fronts on Circulation and Stratification and Mixing Processes in Itumbiara Reservoir (GO): A Hydrodynamic Modelling and Remote Sensing Approach. M.Sc. thesis, National Institute for Space Research, 2012.
- 30 Donn, W. L.: Meteorología, Reverté, Barcelona, 1978.

[Title Page](#)

[Abstract](#)

[Introduction](#)

[Conclusions](#)

[References](#)

[Tables](#)

[Figures](#)



[Back](#)

[Close](#)

[Full Screen / Esc](#)

[Printer-friendly Version](#)

[Interactive Discussion](#)

- Fischer, H. B., List, E. G., Koh, R. C. Y., Imberger, J., and Brooks, N. H.: Mixing in Inland and Coastal Waters, Academic Press, San Diego, 1979.
- Garreaud, R. D.: Cold air incursions over subtropical South America: mean structure and dynamics, *Mon. Weather Rev.*, 128, 2544–2559, 2000.
- 5 Hedger, R. D., Olsen, N. R. B., Malthus, T. J., and Atkinson, P. M.: Coupling remote sensing with computational fluid dynamics modelling to estimate lake chlorophyll *a* concentration, *Remote Sens. Environ.*, 79, 116–122, 2002.
- Hicks, B. B.: A procedure for the formulation of bulk transfer coefficients over water, *Bound.-Lay. Meteorol.*, 8, 515–524, 1975.
- 10 Hodges, B. R., Imberger, J., Saggio, A., and Winters, K. B.: Modeling basin-scale internal waves in a stratified lake, *Limnol. Oceanogr.*, 45, 1603–1620, 2000.
- Hodges, B. R., Laval, B., and Wadzuk, B. M.: Numerical error assessment and a temporal horizon for internal waves in a hydrostatic model, *Ocean Model.*, 13, 44–64, 2006.
- 15 Hondzo, M. and Stefan, H. G.: Long-term lake water quality predictor, *Wat. Res.*, 30, 2835–2852, 1996.
- Imberger, J. and Patterson, J. C.: Physical limnology, *Adv. Appl. Mech.*, 27, 303–475, 1990.
- Jensen, J. R.: Remote Sensing of the Environment: An Earth Resource Perspective, Prentice Hall, Boca Raton, 2006.
- 20 Justice, C. O., Vermote, E., Townshend, J. R. G., Defries, R., Roy, D. P., Hall, D. K., Solomonson, V. V., Privette, J. L., Riggs, G., Strahler, A., Lucht, W., Myneni, R. B., Knyazikhin, Y., Running, S. W., Nemani, R. R., Wan, Z., Huete, A. R., van Leeuwen, W., Wolfe, R. E., Giglio, L., Muller, J.-P., Lewis, P., and Barnsley, M. J.: The Moderate Resolution Imaging Spectroradiometer (MODIS): land remote sensing for global change research, *IEEE T. Geosci. Remote Sens.*, 36, 1228–1247, 1998.
- 25 Krinner, G.: Impact of lakes and wetlands on boreal climate, *J. Geophys. Res.*, 108, 1–18, doi:10.1029/2002JD002597, 2003.
- Kummerow, C., Barnes, W., Kozu, T., Shiue, J., and Simpson, J.: The Tropical Rainfall Measuring Mission (TRMM) sensor package, *J. Atmos. Ocean. Tech.*, 15, 809–817, 1998.
- 30 Kutser, T., Pierson, D. C., Kallio, K. Y., Reinart, A., and Sobek, S.: Mapping lake CDOM by satellite remote sensing, *Remote Sens. Environ.*, 94, 535–540, 2005

Modeling the effects of cold front passages on the heat fluxes

M. P. Curtarelli et al.

[Title Page](#)

[Abstract](#)

[Introduction](#)

[Conclusions](#)

[References](#)

[Tables](#)

[Figures](#)



[Back](#)

[Close](#)

[Full Screen / Esc](#)

[Printer-friendly Version](#)

[Interactive Discussion](#)

Modeling the effects of cold front passages on the heat fluxes

M. P. Curtarelli et al.

[Title Page](#)

[Abstract](#)

[Introduction](#)

[Conclusions](#)

[References](#)

[Tables](#)

[Figures](#)



[Close](#)

[Full Screen / Esc](#)

[Printer-friendly Version](#)

[Interactive Discussion](#)

- León, L. F., Lam, D. C. L., Schertzer, W. M., Swayne, D. A., and Imberger, J.: Towards coupling a 3-D hydrodynamic lake model with the Canadian Regional Climate Model: Simulation on Great Slave Lake, *Environ. Modell. Softw.*, 22, 787–796, 2007.
- Leonard, B. P.: The ULTIMATE conservative difference scheme applied to unsteady one-dimensional advection, *Comput. Method. Appl. M.*, 88, 17–74, 1991.
- Liu, H., Blanken, P. D., Weidinger, T., Nordbo, A., and Vesala, T.: Variability in cold front activities modulating cool-season evaporation from a southern inland water in the USA, *Environ. Res. Lett.*, 6, 1–8, 2011.
- MacIntyre, S., Fram, J. P., Kushner, P. J., Bettez, N. D., O'Brien, W. J., Hobbie, J. E., and Kling, G. W.: Climate-related variations in mixing dynamics in an Alaskan arctic lake, *Limnol. Oceanogr.*, 54, 2401–2417, 2009.
- MacIntyre, S., Romero, J. R., and Kling, G. W.: Spatial-temporal variability in surface layer deepening and lateral advection in an embayment of Lake Victoria, East Africa, *Limnol. Oceanogr.*, 47, 656–671, 2002.
- MacKay, M. D., Neale, P. J., Arp, C. D., De Senerpont Domis, L. N., Fang, X., Gal, G., Jöhnk, K. D., Kirillin, G., Lenters, J. D., Litchman, E., MacIntyre, S., Marsh, P., Melack, J., Mooij, W. M., Peeters, F., Quesada, A., Schladow, S. G., Schmid, M., Spence, C., and Stokesr, S. L.: Modeling lakes and reservoirs in the climate system, *Limnol. Oceanogr.* 54, 2315–2329, 2009.
- Marengo, J. A., Cornejo, A., Satymurty, P., Nobre, C. A., and Sea, W.: Cold surges in tropical and extratropical South America: the strong event in June 1994, *Mon. Weather Rev.* 125, 2759–2786, 1997.
- Marengo, J. A., Ambrizzi, T., Kiladis, G., and Liebmann, B.: Upper-air wave trains over the Pacific Ocean and the wintertime cold surges in tropical-subtropical South America leading to freezes in Southern and Southeast Brazil, *Theor. Appl. Climatol.*, 73, 223–242, 2002.
- Merwade, V.: Effect of spatial trends on interpolation of river bathymetry, *J. Hydrol.*, 371, 169–181, 2009.
- Okely, P., Imberger, J., and Antenucci, J. P.: Processes affecting horizontal mixing and dispersion in Winam Gulf, Lake Victoria, *Limnol. Oceanogr.* 55, 1865–1880, 2010.
- Ostrovsky, I., Yacobi, Y. Z., Walline, P., and Kalikhaman, I.: Seiche-induced mixing: its impact on lake productivity, *Limnol. Oceanogr.*, 41, 323–332, 1996.

- Pacheco, F. S., Assireu, A. T., and Roland, F.: Drifters tracked by Satellite Applied to Freshwater Ecosystems: Study Case in Manso Reservoir, Paréntese, São José dos Campos, 2011.
- Pleskachevsky, A., Gayer, G., Horstmann, J., and Rosenthal, W.: Synergy of satellite remote sensing and numerical modeling for monitoring of suspended particulate matter, *Ocean Dynam.*, 55, 2–9, 2005.
- 5 Pond, S. and Pickard, G. L.: *Introductory Dynamical Oceanography*, Pergamon Press, Oxford, 1983.
- Rajar, R. and Cetina, M.: Hydrodynamic and water quality modelling: an experience, *Ecol. Model.*, 101, 195–207, 1997.
- 10 Rayner, K. N.: Diurnal energetics of a Reservoir Surface Layer, M.Sc. thesis, University of Western Australia, 1981.
- Rouse, W. R., Oswald, C. J., Binyamin, J., Spence, C., Schertzer, W. M., Blanken, P. D., Bussières, N., and Duguay, C. R.: The role of northern lakes in a regional energy balance, *J. Hydrometeorol.* 6, 291–305, 2005.
- 15 Rueda, F. J. and MacIntyre, S.: Flow paths and spatial heterogeneity of stream inflows in a small multibasin lake, *Limnol. Oceanogr.*, 54, 2041–2057, 2009.
- Slater, P. N.: *Remote Sensing: Optics and Optical Systems*, Addison-Wesley, Reading, 1980.
- Spiegel, R. H. and Imberger, J.: The classification of mixed-layer dynamics in lakes of small to medium size, *J. Phys. Oceanogr.*, 10, 1104–1121, 1980.
- 20 Stech, J. L. and Lorenzetti, J. A.: The Response of the south Brazil bight to the passage of wintertime cold fronts, *J. Geophys. Res.*, 97, 9507–9520, 1992.
- Stech, J. L., Lima, I. B. T., Novo, E. M. L. M., Silva, C. M., Assireu, A. T., Lorenzetti, J. A., Carvalho, J. C., Barbosa, C. C. F., and Rosa, R. R.: Telemetric monitoring system for meteorological and limnological data acquisition, *Verh. Internat. Verein. Limnol.*, 29, 1747–1750, 25 2006.
- Tranvik, L. J., Downing, J. A., Cotner, J. B., Loiselle, S. A., Striegl, R. G., Ballatore, T. J., Dillon, P., Finlay, K., Fortino, K., Knoll, L. B., Kortelainen, P. L., Kutser, T., Larsen, S., Laurion, I., Leech, D. M., McCallister, S. L., McKnight, D. M., Melack, J. M., Overholt, E., Porter, J. A., Prairie, Y., Renwick, W. H., Roland, F., Sherman, B. S., Schindler, D. W., Sobek, S., Tremblay, A., Vanni, M. J., Verschoor, A. M., von Wachenfeldt, E., and Weyhenmeyera, G. A.: Lakes and reservoirs as regulators of carbon cycling and climate, *Limnol. Oceanogr.*, 54, 30 2298–2314, 2009.

Modeling the effects of cold front passages on the heat fluxes

M. P. Curtarelli et al.

[Title Page](#)

[Abstract](#)

[Introduction](#)

[Conclusions](#)

[References](#)

[Tables](#)

[Figures](#)

◀

▶

◀

▶

[Back](#)

[Close](#)

[Full Screen / Esc](#)

[Printer-friendly Version](#)

[Interactive Discussion](#)



**Modeling the effects
of cold front
passages on the heat
fluxes**

M. P. Curtarelli et al.

[Title Page](#)[Abstract](#)[Introduction](#)[Conclusions](#)[References](#)[Tables](#)[Figures](#)[◀](#)[▶](#)[◀](#)[▶](#)[Back](#)[Close](#)[Full Screen / Esc](#)[Printer-friendly Version](#)[Interactive Discussion](#)

- Vidal, J., Rueda, F. J., and Casamitjana, X.: The seasonal evolution of high vertical-mode internal waves in a deep reservoir, *Limnol. Oceanogr.*, 52, 2656–2667, 2007.
- Verburg, P. and Antenucci, J. P.: Persistent unstable atmospheric boundary layer enhances sensible and latent heat loss in a tropical great lake: Lake Tanganyika, *J. Geophys. Res.*, 115, 1–13, 2010.
- Wan, Z.: New refinements and validation of the MODIS land-surface temperature/emissivity products, *Remote Sens. Environ.*, 12, 59–74, 2008.
- Wüest, A. and Lorke, A.: Small-scale hydrodynamics, *Annu. Rev. Fluid Mech.*, 35, 373–412, 2003.

Modeling the effects of cold front passages on the heat fluxes

M. P. Curtarelli et al.

Table 1. Technical specification of the SIMA sensors.

Sensor	Manufacturer	Range	Accuracy	Height
Air temperature	Rotronic	–4 to 60 °C	±0.3 °C	3
Wind speed	Young	0 to 100 ms ^{−1}	±0.3 ms ^{−1}	3
Wind direction	Young	0 to 360°	±3°	3
Relative humidity	Rotronic	0 to 100 %	±1 %	3
Shortwave radiation	Novalynx	0 to 1500 W m ^{−2}	< 1 W m ^{−2}	3
Barometric pressure	Vaisala	800 to 1060 hPa	±0.3 hPa	3

[Title Page](#)

[Abstract](#)

[Introduction](#)

[Conclusions](#)

[References](#)

[Tables](#)

[Figures](#)



[Back](#)

[Close](#)

[Full Screen / Esc](#)

[Printer-friendly Version](#)

[Interactive Discussion](#)

Modeling the effects of cold front passages on the heat fluxes

M. P. Curtarelli et al.

Table 2. Summary of weather conditions during the cold front passages over the Itumbiara Reservoir. Drop in air temperature (ΔT_a), maximum wind intensity (U_{\max}), preferential wind direction, relative humidity variation (ΔRH) and accumulated precipitation (P).

Cold front ID	Date	ΔT_a (°C)	U_{\max} (m s ⁻¹)	Wind Direction	ΔRH (%)	P (mm)
F1	9 May 2010–10 May 2010	5.2	7.1	From NE to SW	30.9	0
F2	12 May 2010–13 May 2010	3.8	6.5	From NE to SW	55.7	0
F3	18 May 2010–20 May 2010	3.4	8.6	From NE to S	54.1	4.4
F4	30 May 2010–1 Jul 2010	3.1	8.8	From NE to S	63.9	73.2
F5	4 Jul 2010–7 Jul 2010	4.3	7.2	From NE to S	57.6	16.7

- [Title Page](#)
- [Abstract](#) [Introduction](#)
- [Conclusions](#) [References](#)
- [Tables](#) [Figures](#)
- [◀](#) [▶](#)
- [◀](#) [▶](#)
- [Back](#) [Close](#)
- [Full Screen / Esc](#)
- [Printer-friendly Version](#)
- [Interactive Discussion](#)

Table 3. Mean Absolute Error (MAE) and RMSE of the simulated temperature at the S1 and S2 stations.

Depth sampled (m)	S1				S2			
	MAE (°C)	MAE (%)	RMSE (°C)	RMSE (%)	MAE (°C)	MAE (%)	RMSE (°C)	RMSE (%)
1.5	0.29	1.12	0.32	1.22	—	—	—	—
5	0.30	1.18	0.33	1.28	0.36	1.4	0.39	1.49
12	0.27	1.06	0.30	1.15	0.36	1.42	0.39	1.51
20	0.26	1.03	0.29	1.11	0.65	2.53	0.75	2.89
40	0.39	1.49	0.45	1.74	—	—	—	—
Average	0.30	1.18	0.34	1.3	0.46	1.78	0.51	1.96



Modeling the effects of cold front passages on the heat fluxes

M. P. Curtarelli et al.

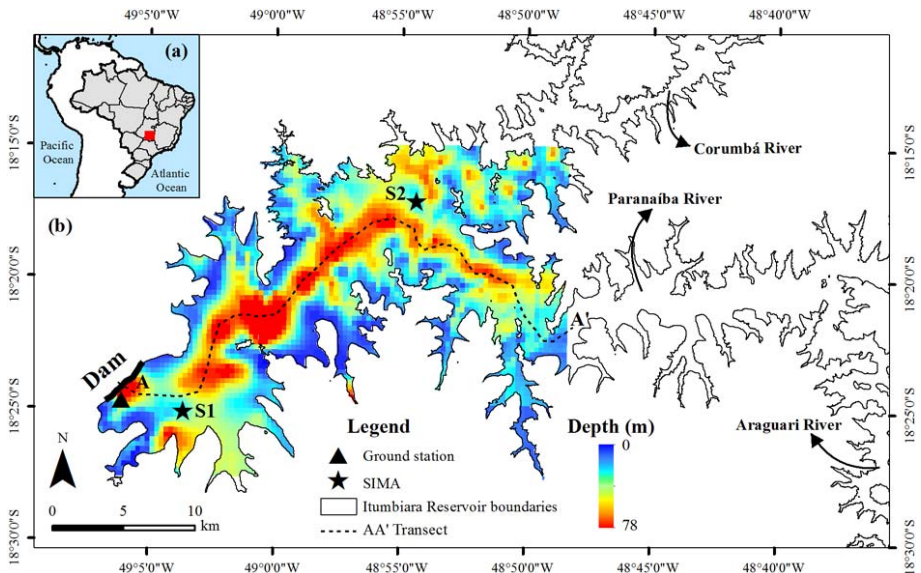


Fig. 1. Location of the Itumbiara Reservoir (red square) in Central Brazil (**a**) and its detailed boundaries and bathymetry (**b**).

Title Page

Abstract

Introduction

Conclusion

References

Tables

Figures



Back

Close

Full Screen / Esc

[Printer-friendly Version](#)

Interactive Discussion

Modeling the effects of cold front passages on the heat fluxes

M. P. Curtarelli et al.

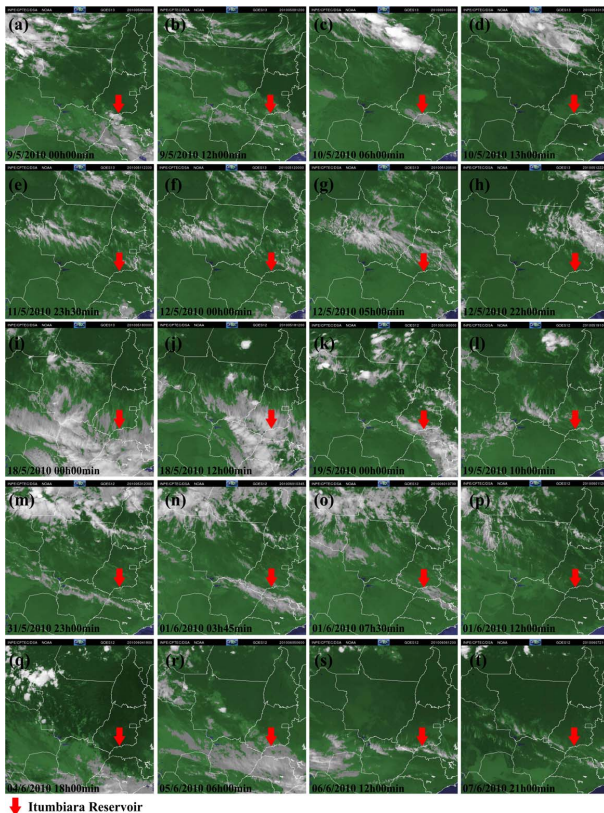


Fig. 2. Cloudiness associated with cold front passages over the Itumbiara Reservoir observed by the Geostationary Observational Environmental Satellite (GOES). False color composites (R2G3B1) during the F1 (**a–d**), F2 (**e–h**), F3 (**i–l**), F4 (**m–p**) and F5 (**q–t**) passages.

Modeling the effects of cold front passages on the heat fluxes

M. P. Curtarelli et al.

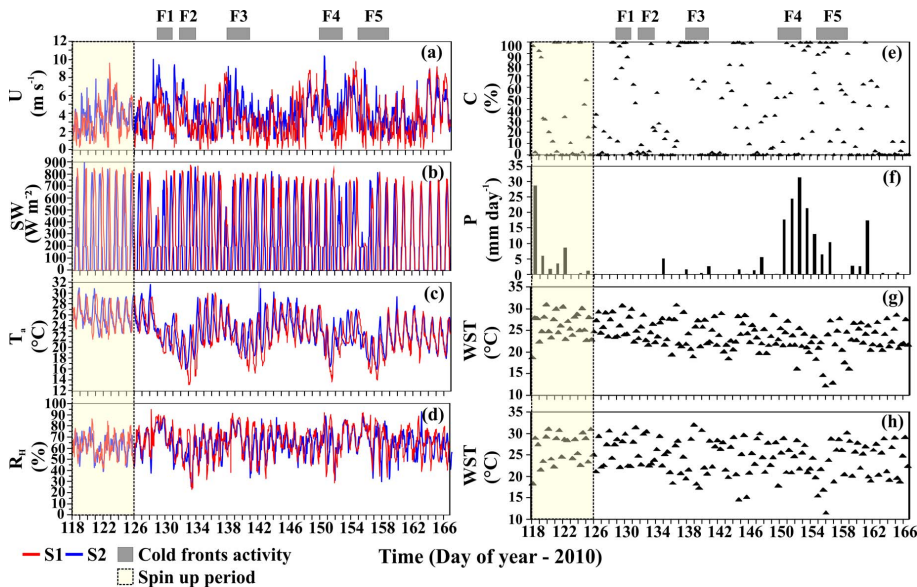


Fig. 3. Wind speed (a), shortwave radiation (b), air temperature (c), relative humidity (d), cloud cover (e), precipitation rate (f), WST at the Paranaíba inflow (g) and WST at the Corumbá inflow (h) time series used to enforce the hydrodynamic model.

- [Title Page](#)
- [Abstract](#) [Introduction](#)
- [Conclusions](#) [References](#)
- [Tables](#) [Figures](#)
- [◀](#) [▶](#)
- [◀](#) [▶](#)
- [Back](#) [Close](#)
- [Full Screen / Esc](#)

[Printer-friendly Version](#)

[Interactive Discussion](#)

Modeling the effects of cold front passages on the heat fluxes

M. P. Curtarelli et al.

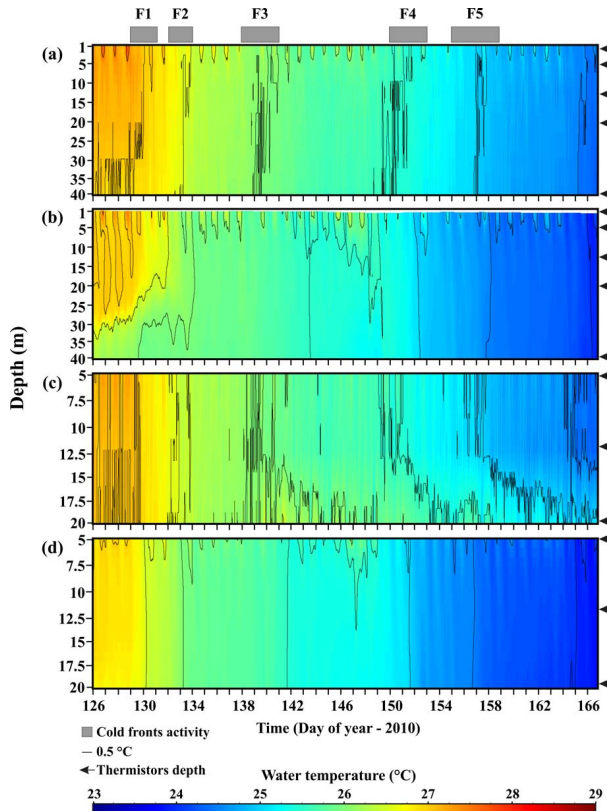


Fig. 4. Observed (**a**) and modeled (**b**) water temperature near the dam (station S1); observed (**c**) and modeled (**d**) water temperature in the river-reservoir transition zone (station S2).

Title Page

Abstract

Introduction

Conclusion:

References

Tables

Figures



Back

Close

Full Screen / Esc

Interactive Discussion

**Modeling the effects
of cold front
passages on the heat
fluxes**

M. P. Curtarelli et al.

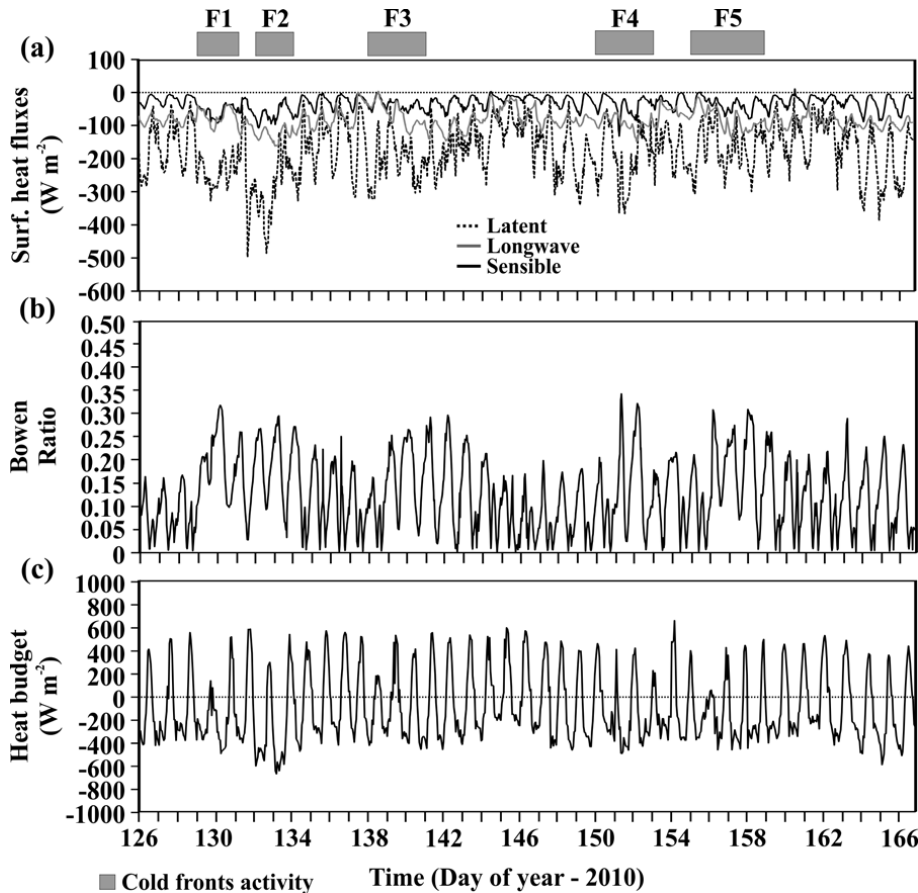


Fig. 5. Surface heat fluxes **(a)**, Bowen ratio **(b)** and total heat budget **(c)** of the Itumbiara Reservoir.

Modeling the effects of cold front passages on the heat fluxes

M. P. Curtarelli et al.

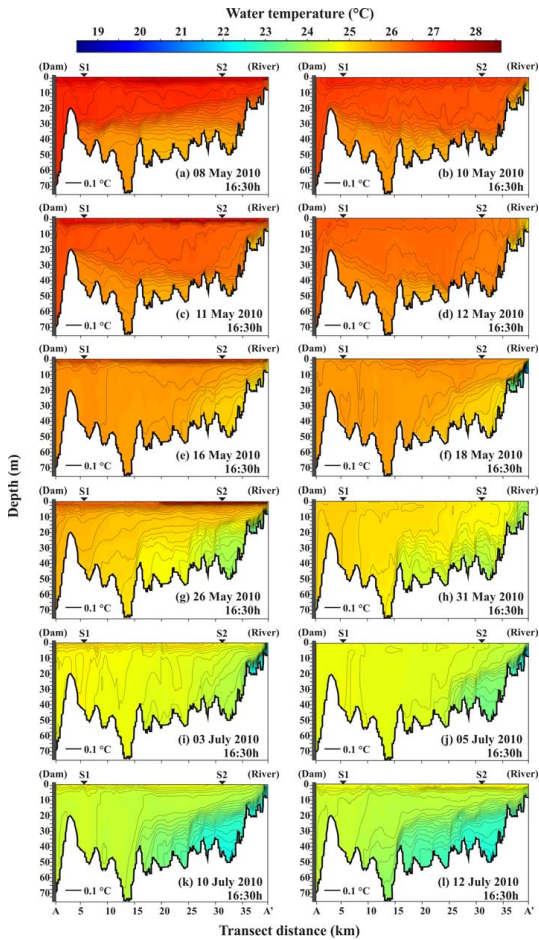


Fig. 6. Changes in the thermal structure of the Itumbiara Reservoir along its longitudinal transect (a–l).

Discussion Paper | Discussion Paper

[Title Page](#)

[Abstract](#)

[Introduction](#)

[Conclusions](#)

[References](#)

[Tables](#)

[Figures](#)



[Back](#)

[Close](#)

[Full Screen / Esc](#)

[Printer-friendly Version](#)

[Interactive Discussion](#)

Modeling the effects of cold front passages on the heat fluxes

M. P. Curtarelli et al.

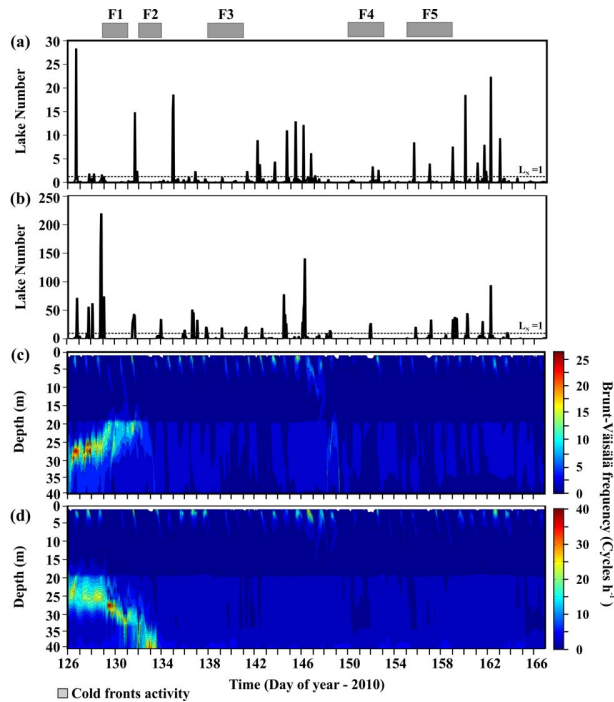


Fig. 7. Lake number near the dam (**a**) and in the river–reservoir transition zone (**b**); Brunt–Väisälä frequency near the dam (**c**) and in the river–reservoir transition zone (**d**).